

Chapter 19

Millimeter-Wave and Terahertz Imaging in Security Applications

Arttu Luukanen, Roger Appleby, Mike Kemp and Neil Salmon

Abstract The relatively short wavelength of mm-wave and THz radiation coupled with good transmission through many dielectric materials allows images to be formed of concealed objects. This chapter gives an overview of the detectors, their associated circuitry, and system developments over the past 10 years, focussing on personnel security screening. We will discuss the phenomenology of imaging at these wavelengths, introduce the reader to the basic architectures being used and developed for image forming instruments, show examples of systems, and also discuss the feasibility of spectroscopic THz imaging for security screening applications.

19.1 Introduction

Electromagnetic radiation in the millimeter to terahertz band (30 GHz to 10 THz) is nonionizing and therefore its use is free from public health concerns associated with the use of frequent exposure to nuclear radiation and X-rays. One of the first imaging systems was developed by the Royal Radar Establishment in the 1950s [1], a rather remarkable feat considering that the system was based on thermionic valve

A. Luukanen (✉) · R. Appleby
MilliLab co VTT Technical Research Centre of Finland, Finland, Europe
e-mail: arttu.luukanen@vtt.fi

R. Appleby
Queen's University Belfast, Cambridge, UK
e-mail: r.appleby@qub.ac.uk

M. Kemp
Iconal Technology Limited, Cambridge, UK
e-mail: mike.kemp@iconal.com

N. Salmon
MMW Sensors Ltd, Manchester, UK
e-mail: Neil.Salmon@MMW-Sensors.com

technology. Later in the 1970s, passive millimeter-wave (MMW) imaging in the band 100–300 GHz was investigated using semiconductor technology, as a means to detect nuclear radiation shielding materials and concealed explosives [2, 3]. During the 1980s and the early 1990s a better understanding of the phenomenology of passive MMW imaging was developed, due to the increasing number of proof of concept imaging systems that had been designed and operated in the atmospheric transmission windows and absorption bands in this region. The motivation for much of this work was to demonstrate the ability of systems in this waveband to detect and recognize metal and non-metallic threats concealed under clothing. In the mid to late 1990s a number of video rate imaging systems was developed at 35 GHz and 90 GHz and from 2000 until 2011 demonstration systems were developed to 1 THz and beyond, spurred on by the September 11th event in 2001. Some of the prototypes have been commercialized and are currently in use or under evaluation.

This chapter provides an overview of the imaging technologies that are being developed and deployed for security screening applications.

19.2 Phenomenology of Security Screening

Imaging for security applications can either be achieved passively where the natural radiation emitted and reflected by the object of interest is used or actively where a transmitter provides illumination and the image is formed from this reflected light.

In this section both passive and active imaging are described, followed by the properties of the atmosphere and relevant materials.

19.2.1 System Performance Metrics in Passive MMW Imaging

Security screening aims to detect, recognise and identify threats carried on people with a high probability and a low false alarm rate, ideally at video rates on moving subjects. The detection is based on the measurement of minute spatial variations in the natural thermal (black body) radiation emitted by the target. Systems required to do this must have good receiver operating characteristics [4] and to achieve this it is important to understand the basic performance metrics of an imager, how contrast in an image arises, and the phenomenology of imaging in various scenarios.

The noise equivalent power (NEP) of a detector relates to post-detection signal-to-noise ratio as $SNR = P_{in} (\text{NEP}_{\text{sys}} \sqrt{\Delta f_{\text{ENBW}}})^{-1}$, where Δf_{ENBW} is the post-detection effective noise bandwidth for data collection in a single pixel in the image.

The noise equivalent temperature difference (NETD), of a passive MMW imaging system is given by the radiometer equation Eq. 19.1, where T_A is the antenna temperature (the radiation temperature of the pixel being viewed), T_R is the receiver noise temperature, and $\Delta \nu_{\text{RF}}$ is the radiometric bandwidth [5]. Often mechanical scanning

of N_i image pixels with N_{rec} receivers is utilized which reduces the per-pixel dwell time and increases $\Delta f_{\text{ENBW}} \propto N_i/N_{\text{rec}}$. This leads to tradeoffs in systems designs between the number of receiver channels in the focal plane array, the field of view (FOV), the noise, and the image update frame rate.

$$\text{NETD}_{\text{sys}} = (T_A + T_R) \sqrt{\frac{\Delta f_{\text{ENBW}}}{\Delta \nu_{\text{RF}}}} = \frac{\text{NEP}_{\text{sys}} \sqrt{\Delta f_{\text{ENBW}}}}{k_B \Delta \nu_{\text{RF}}}. \quad (19.1)$$

The angular resolution $\Delta\theta$, in a passive MMW image is set by the diffraction limit associated with the size of the primary optics aperture D , this being given by $\Delta\theta \sim \lambda/D$ where λ is the radiation wavelength.

19.2.2 Contrast in Passive MMW Imagers

The radiometric contrast between an object and its background is governed by their different radiation temperatures. The radiation temperature T_{RAD} of any part of the subject is described to a first approximation by Eq. 19.2, where T_{ILL} is the illuminating radiation temperature, and T_{SUB} and Γ_{SUB} are the subject thermodynamic temperature and reflectance, respectively. The illuminating temperatures will be dependent on the environment, while the reflectances are dependent on material properties. Metal has a reflectance of 100% and human skin a reflectance of between 5% and 40%, depending on frequency, incidence angle, and body region. For normal incidence the reflectance in going from one medium into a second is given by Eq. 19.3, where n is the complex refractive index of the media. For air, the refractive index, n_1 , is unity.

$$T_{\text{RAD}} = T_{\text{ILL}} \Gamma_{\text{SUB}} + T_{\text{SUB}} (1 - \Gamma_{\text{SUB}}), \quad (19.2)$$

$$\Gamma = \left(\frac{n_1 - n_2}{n_1 + n_2} \right)^2. \quad (19.3)$$

More complex models exist for the reflection from multiple layers of clothing and non-metallic threats against the body [6]. Signatures then become dependent upon the reflectance, Γ , emissivity e , and transmittance, γ of the constituent materials, which sum to unity as indicated in Eq. 19.4. The absorption coefficient α of radiation in these materials is determined by the imaginary part of the refractive index n'' and is given by Eq. 19.5. Furthermore, in moving up into the submillimeter-wave (SMMW) band, scattering plays an increasing role in the blurring of the edge of objects. In scenarios where thin layers of energetic materials are placed close to the body internal reflections may need to be accounted for. Details of the properties of clothing, skin, and energetic materials are provided in Sect. 19.2.7 below.

$$\Gamma + e + \gamma = 1, \quad (19.4)$$

$$\alpha = \frac{4\pi}{\lambda} n''. \quad (19.5)$$

For stand-off security screening, particularly at the higher frequencies, absorption and emission from the atmosphere will appreciably reduce the contrast in images. This, together with the absorption and scattering in the overlying layers of clothing, limits the maximum usable upper frequency. The radiation temperature T_R of the subject measured at the imager location is given by Eq. 19.6, where T_0 is the atmospheric temperature and τ is the optical depth of the atmosphere between the subject and the imager, this being the line integral of the atmospheric absorption, α , along the line of sight, as given in Eq. 19.7. Atmospheric attenuation in the MMW and SMMW band is discussed below.

$$T_R = T_{\text{RAD}} e^{-\tau} + T_0 (1 - e^{-\tau}), \quad (19.6)$$

$$\tau = \int_{\text{IMAGER}}^{\text{SUBJECT}} \alpha \, ds. \quad (19.7)$$

The diffraction limit, $\Delta\theta \sim \lambda/D$, limits the use of lower cost and more mature technology at the lower MMW frequencies to short-range ($\lesssim 5$ m) or portal applications only. For the same reason, operation well into the SMMW band is necessary for stand-off security screening in order to achieve the necessary spatial resolution. The upper frequency limit for stand-off systems is governed by the reduction in contrast of threats, which is determined by the extinction (absorption and scattering) in overlying clothing and the atmosphere.

19.2.3 Passive MMW Imaging Phenomenology

Illumination of subjects is an important factor that determines the phenomenology in passive MMW imaging. The natural illumination in the millimeter wave band arises from a multitude of spatially incoherent modes of thermal (Planck) radiation, much like in the visible part of the spectrum. For this reason passive MMW images have a very natural appearance and are easy to interpret, which is a great asset in security screening. A convention of dark shades for high radiation temperatures gives the ground a darker appearance and the sky a lighter appearance, resulting in images similar in appearance to those of visible monochromes. This is the black-is-“hot” convention. However, the reverse, white-is-“hot” convention, is also used.

Indoor images taken in the millimeter and sub-millimeter wave band show phenomenology associated with uniform illumination. This is because the radiation temperature of emission inside a building is almost isotropic and held at a level determined by the indoor building temperature. In these scenarios the contrast in

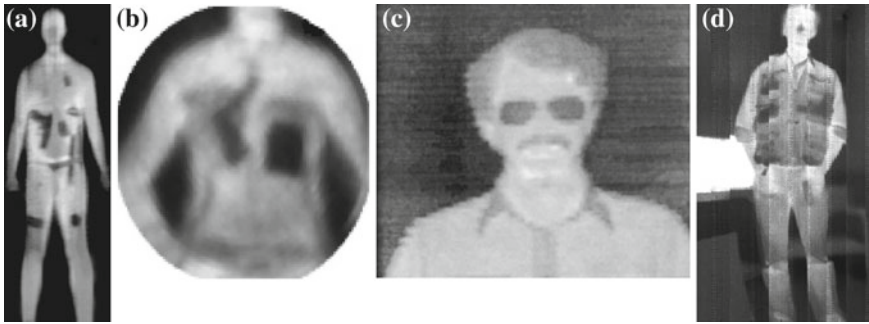


Fig. 19.1 Passive indoor imaging at (a) 94 GHz [7], (b) 350 GHz [8], (c) 600 GHz (wearing glasses) [9] and (d) broadband (0.2 – 1 THz) [10]. The increase in the visibility of clothing is apparent when moving from the lower to the higher frequencies, by the change in contrast of shirt collars and seams (White-is-“hot”)

the image arises from the difference between the illumination from the building and that from the human body, which may be typically ~ 20 °C. An example of such imagery is shown in Fig. 19.1, where the body appears at a fairly uniform radiation temperature and concealed objects appear at lower radiation temperatures. This phenomenology is also characteristic of outdoor imagery at the higher frequencies (>300 GHz) and in the atmospheric absorption bands, as the illuminating radiation temperature is almost isotropic, a consequence of the high atmospheric attenuation. In these regimes contrast over the subject is largely a result of differences in emissivity and physical temperature, rather than reflectivity.

Outdoor images taken in the atmospheric transmission windows at 35 GHz and 94 GHz have the characteristic features associated with relatively “cold” illuminating radiation from the sky and “warm” radiation from the ground. The sky radiation temperature will typically be in the region 20–180 K and dependent on frequency, zenith angle and weather conditions. Illuminating radiation from below is generally much “warmer,” typically in the region 250–300 K and dependent on the ground material. This gives rise to characteristic features associated with “cold” radiation being reflected from upward facing body surfaces, such as the shoulders and chest regions and “warm” radiation being reflected from downward facing surfaces, as illustrated in Fig. 19.2a. This illumination can also enhance the contrast of highly reflective items such as those made of metal.

Phenomenology associated with the frequency variation in the attenuation of clothing and hair is also recognized. As frequency increases, the attenuation of hair and clothing rises, due to increased absorption and scattering, as the wavelength approaches that of clothing weave size and hair strand diameter (~ 100 μm). This is illustrated in Fig. 19.2b, which shows a 94 GHz image of a person with a full head of hair. None of the hair is visible in the image. This is to be compared with the passive images of a persons at ~ 600 GHz Fig. 19.1, where hair is very apparent.

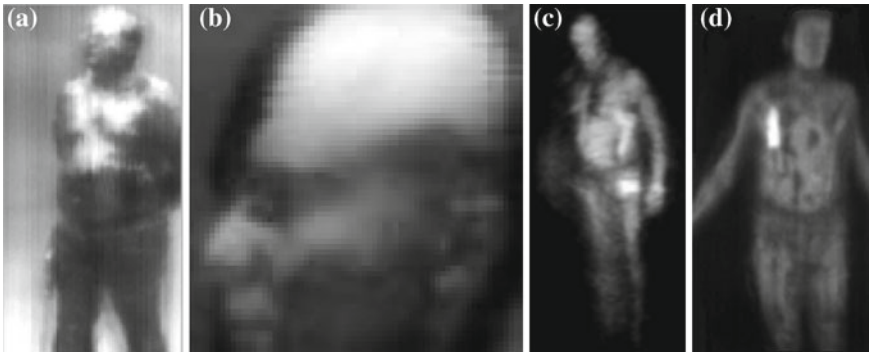


Fig. 19.2 **a** and **b**: Passive outdoor images at 94 GHz. “Cold” radiation from the sky is reflected by upward facing body surfaces, generating contrast. No hair is discernable in these images, even though the person has a full head of hair [12]. (Black-is-“hot”). Portal images **c** using spatially incoherent illumination at 35 GHz from a noise source inside a mode scrambling cavity [13] and **d** at 94 GHz from thermally warm panels illustrating concealed threats as white [14]. (White-is-“hot”)



Fig. 19.3 (Left) Still frames from 10 fps passive mm-wave video imagery (MMW and visible with privacy overlay algorithm) from the Millivision Portal 350 system. (Right) The user interface of the Millivision Walk-by 350 system. [64]

Polarization has not been shown to be a powerful discriminator in passive MMW imaging, as the degree of linear polarization is generally below 20% and that of circular polarization below 1% [11]. For this reason systems tend to operate with just a single polarization.

Artificial illumination schemes arose out of attempts to increase the image contrast in indoor screening scenarios. Spatially and temporally incoherent illumination was generated using electronic noise sources and mode stirrers, or heated absorbers acting as radiators, emulating outdoor illumination, but in a more controlled fashion. As the illumination is spatially incoherent, the phenomenology of this type of imaging

has more in common with passive MMW imaging than radar imaging, (discussed below) and is therefore described here. Images from security screening portals that use this technique at 35 GHz and 94 GHz are shown in Fig. 19.2c and d as well as in Fig. 19.3.

19.2.4 Active (Coherent) Millimeter Wave Imaging

Active sensing in the millimeter wave band was a natural progression of radar techniques used at the lower frequencies. The benefit of using an active technique is that a controlled stimulus can be used to probe a region, which may be an area that has little measurable passive signature, and that range gating can be used. The use of coherent detection methods allows for greatly enhanced signal-to-noise ratio. The central governing equation here is the radar equation, $P_R = P_T G_T A_R \sigma / [(4\pi)^2 R_R^2 R_T^2]$, which gives the level of power returned from a subject (less than or equal to the beam width of the antenna), P_R , for a given transmit power, P_T , where G_T is the gain of the transmit antenna, A_R is the area of the receiver antenna, R_T is the transmitter to subject range, R_R is the receiver to subject range, and σ is the radar scattering cross-sectional area of the subject [15]. This R^4 dependence can reduce to R^2 when the radar transmits and receives using a single antenna [19].

As the total noise in a receiver system is proportional to the radio frequency bandwidth, the highest signal-to-noise ratios are achieved when the active source transmits in the narrowest possible spectral bandwidth and the receiver bandwidth is then tuned to this. This is almost the reverse of imaging radiometry, where wider radiation bandwidths generate higher signal-to-noise ratios.

In further contrast to passive MMW imaging, the illumination needs to be coherent over the signal integration time. This requires the source to be both spatially and temporally coherent. However, narrow bandwidths introduce clutter in the form of speckle, etalon, and multi-path effects, making threats difficult to discriminate. The use of radar techniques, for example range gating, can reduce the scatter from overlying layers of clothing to reveal concealed threats beneath. The unambiguous range resolution, ΔR , in radars is inversely related to the bandwidth of the modulation, $\Delta\nu_{RF}$, and is given by $\Delta R = c / (2\Delta\nu_{RF})$, where c is the speed of light. However, increasing the bandwidth requires greater powers to be transmitted, particularly if centimeter- scale range resolution is required for threat discrimination.

For attenuation of the illuminating radiation in the atmosphere and in clothing, similar arguments apply to those of passive systems. However, an active system is less vulnerable to the extinction by clothing and the atmosphere thanks to their larger dynamic range. This means they can generally operate out to greater ranges and at higher frequencies than the passive counterparts.

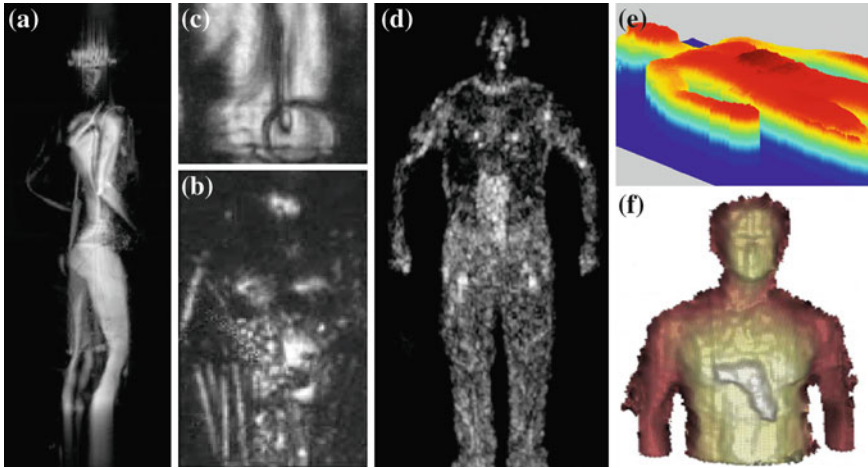


Fig. 19.4 **a** Portal active imaging at 24–34 GHz of a mannequin [16] and **b** at 24 GHz of a person carrying concealed weapons, using active coherent illumination [17]. **c** A disk of simulant energetic material is revealed by scattering from edges, while the bulk material is transparent. *Stand-off* active imaging at 350 GHz **d**, **e** [18] and at **f** 600 GHz using coherent illumination [19]. A concealed package on the stomach area is recognized by the contrast in the 2D image **d** and by its 3D form using range gating **e**. Similar range gating discriminates characteristic form at 600 GHz **f**.

19.2.5 Active Millimeter Wave Imaging Phenomenology

In active imaging contrast over a subject is very much dependent on the reflectivity and scattering from materials and the body. Furthermore, as the technique is not dependent on illumination from external sources, there is little difference between indoor and outdoor imaging phenomenology.

Portal imaging systems operating at the lower frequencies (24–35 GHz) are capable of generating detailed full three-dimensional images of a subject, as illustrated in Fig. 19.4. At the low frequencies the difference in reflectivity between energetic materials on skin and the skin by itself can be small; however, the presence of these threats may be detected by the scattering from their edges.

Stand-off imaging systems operating at the higher frequencies are capable of generating images at range with good spatial resolution as illustrated by systems operating at 350 GHz and 600 GHz in Fig. 19.4d–f. Concealed objects are apparent in the two-dimensional images, but further discrimination in three dimensions may be provided by range gating. This is illustrated in the figure, where a depth profile of reflection over the front area of the body may be created to reveal concealed threats. At higher frequencies it becomes increasingly difficult to discriminate concealed threats in a purely two dimensional image, due to the increased scattering and the reduction of signal level by the overlying clothing.

Scattering as a phenomenon is very apparent in active imaging in the submillimeter wave band, as illustrated by the image of a person's face and hair in Fig. 19.5.

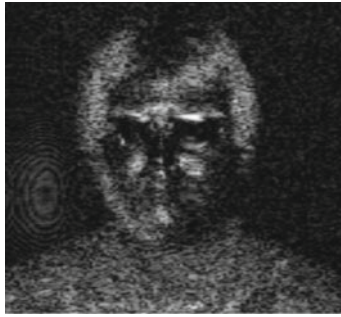


Fig. 19.5 Stand-off active imaging using illumination at 640GHz (D. Petkie, Wright State University, 2011). The left-side of the face has a couple of days' growth of stubble compared to the right-hand side, which is clean shaven. This is apparent in the image and may be expected, as hair strand diameter is $\sim 100\ \mu\text{m}$ and growth rate is $\sim 300\ \mu\text{m}$ per day, which are appreciable fractions of the $\sim 470\ \mu\text{m}$ wavelength

Although the person appears to have a full head of hair in the visible band, there is little millimeter wave signal return from the top of the head, but a significant amount of scattering from a relatively short growth of stubble.

Polarization offers powerful capabilities in active systems as it can be used to discriminate between plane reflectors and edges. Plane reflectors change the handedness of circular polarization, i.e., right-hand circular polarization is reflected to left-hand circular polarization. Detecting right-handed returns therefore rejects the plane surface reflections, emphasizing the scatter from edges, as they have a predominantly linear polarization component. In addition, multi-path effects can also be discriminated by exploiting circularly polarized radiation and these effects are discussed more fully in [20]. Generally, full polarimetric systems, operating in transmit and receive, have the potential to reveal a multitude of detail about concealed threats.

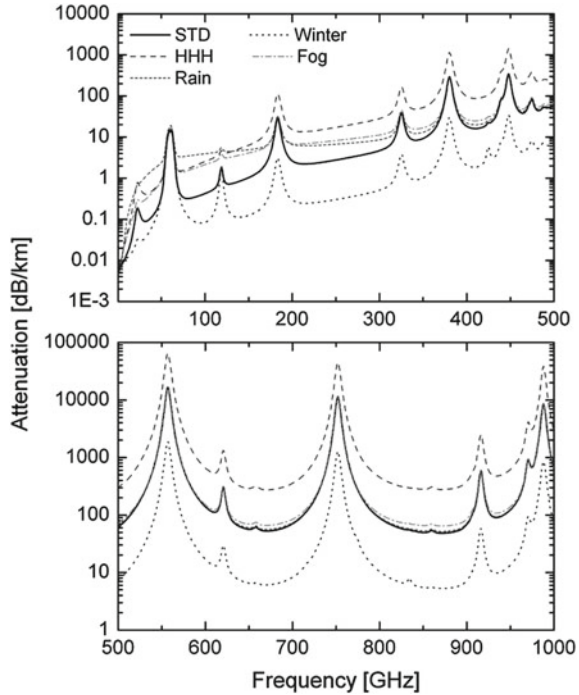
19.2.6 Atmospheric Transmission

The atmospheric attenuation up to 1 THz is shown for a variety of weather conditions in Fig. 19.6. The attenuation rises with frequency and there are regions of high attenuation due to the rotational absorption lines of molecular oxygen and water vapor.

19.2.7 Material Properties

In an imaging system designed for security screening, the observed image is dependent on the optical properties of clothing, metal, and skin, and can be described

Fig. 19.6 Atmospheric attenuation in the band up to 1 THz for various weather conditions [21]: STD—Standard US atmosphere; HHH—Hot and humid; Winter —10°C, Fog—100 m visibility, Rain—4 mm/hr



in terms of their transmittance γ , emissivity e , and reflectance Γ , as shown in Table 19.1. More detailed information can be found on the transmission of clothing in Reference [22] and on the millimeter wave properties of energetic materials in References [23–26]. A spectrum of the absorption coefficient and reflectance of these materials are presented in Fig. 19.19. From the table it is clear that metal has a reflectivity of unity, which is frequency independent. Zirconia, from which ceramic knives are made, is also a strong reflector. The emissivity of skin increases with frequency and the transmission of clothing decreases with frequency. Many explosives have a high transmission at 100 GHz, which decreases as the frequency is increased.

As can be seen in the table, a 5-mm thick sample will have a small contrast against the body, the transmittance being zero in this case, as no radiation is passed through the body. However, some energetic mixtures generally have higher emissivities, giving them a larger signature. Many objects, including clothing and formulated explosives, often have fiber, which scatters the incident radiation. This will cause radiation which would normally be transmitted or reflected to be scattered over a wider angle, changing the level of signal return and modifying the local illumination of objects. The effect is a smearing out of the spatial details of the objects.

Moisture in the form of human body perspiration and its effect on clothing transmission needs to be considered when comparing signatures from real subjects with simulations. The large dipole moment on the water molecule means that even small

Table 19.1 Optical properties of 5 mm thick energetic materials, skin, metal, denim, *t*-shirt [27] and leather [22]

Frequency (GHz)	Emissivity (ϵ)			Reflectance (Γ)			Transmittance (γ)		
	100	500	1,000	100	500	1,000	100	500	1,000
Nitro based energetic compounds on skin	0.76	0.95	0.94	0.24	0.05	0.06	0	0	0
Metal	0	0	0	1	1	1	0	0	0
Ceramic (Zirconia)	0	0	0	0.9	0.9	0.9	0	0	0
Skin	0.65	0.91	0.93	0.35	0.09	0.07	0	0	0
Denim	0.09	0.49	0.85	0.01	0.01	0.05	0.9	0.5	0.1
Tee-shirt	0.04	0.2	0.3	0	0	0.05	0.96	0.8	0.65
Leather							0.8	0.42	0.09

amounts of water can significantly increase the attenuation in clothing, which is apparent in imagery. However, simulations may be based on optimistically high levels of transmission, arising from laboratory measurements of relatively dry clothing samples.

19.3 Imaging System Design Overview

The engineers designing passive image forming systems for mm-wave to THz frequencies typically face several challenges:

- “Detector-starvation”—High cost of detectors, an economic limit set by the small number of uses in this band.
- Wide field-of-view coverage, a requirement set by the end-user.
- Diffraction-limited optical systems are compulsory, as end-users require systems to be compact requiring the aperture to be minimized.
- Passive systems are also prone to “Signal-starvation”—Low signal levels at detectors, a fundamental limit set by the Planck emission formula.

For passive systems the Planck black body emission formula indicates the signal power at 94 GHz corresponding to a 1 K level of sensitivity at an ambient temperature of 300 K is ~ 260 fW (in single mode,¹ 20% relative bandwidth). Compare this with the single-mode power available in the LWIR (8–12 μ m) of ~ 30 pW, i.e. some two orders of magnitude more signal power is present in the thermal infrared. Active systems, on the other hand, may suffer less from low signal levels, as it may be possible to use higher transmit powers.

The high costs of detectors can to some extent be off-set by using mechanical scanning to scan the subject with a single or small number of detectors. However, due to the long wavelength of the radiation, the optics are often large (~ 1 m diameter)

¹ One polarization, one spatial mode.

and making reliable, vibration-free scanning systems for near real-time frame refresh rates (≤ 30 Hz) a significant engineering challenge.

A specialized methodology, used in the design of MMW to THz systems, is referred to as or *quasi-optics* or *Gaussian optics*, a branch of optics where diffraction within an instrument is considerable and the optical beam, by design, has a Gaussian intensity distribution [28, 29]. The simultaneous requirements for large FOV and diffraction limited performance across the FOV poses a challenge to the design of the optics, as optical aberrations increase rapidly when moving away from the paraxial region to the off-axis beams.

As an alternative to focal plane image formation, pupil-plane image formation can also be employed [30–32]. In a focal plane imaging system the detectors are located after the image forming optics, while in a pupil-plane system image formation takes place in either electronics or optics (after upconversion). Prototypes are still at the design stage but could potentially be used to build an imager of planar geometry which could be fixed to a wall.

An interesting combination of electronic and optical image formation is the use of adaptive holograms: Utilizing well-established methods of holography, one can design a reflective (or transmissive) surfaces with a phase or amplitude pattern that corresponds to the interference pattern of the illuminating input beam (of a transceiver) and the transferred (output) beam, focussed to a given location in the target space. Phase holography is preferable from the standpoint of efficiency, as an amplitude hologram necessarily loses a substantial fraction of the input power. One approach that has been recently developed [17] employs a large array of patch antennas, each of which is connected to a p-i-n phase shifter. The phase shifter can be a p-i-n diode, liquid crystal polymer (LCP), or RFMEMS phase shifter [33, 34]. Even the use of optical excitation in a photoconductor has been investigated [35]. The benefits of this so-called “reflectarray” beam steering approach are numerous, including low loss (since no lengthy feeding networks are required), scalability, adaptability, and the strong leveraging effect through the utilization of digital pattern generation techniques.

19.4 Detector Technologies

In this section we give a brief overview of coherent and incoherent detection methods for MMW and THz imaging. For more a comprehensive treatment we refer the reader to excellent reviews [36–38].

A detector is a device that rectifies the electric fields of an incoming wave, converting its power into an rms voltage (or current), with an integration time commensurate with application requirements. In the process of rectification the phase of the wave is lost and as such they are only suitable for incoherent detection systems. A mixer on the other hand multiplies the electric field of the incoming wave with a locally generated field, shifting the wave either up or down in frequency. In the process of mixing both the phase and amplitude of the original incoming wave are retained and

can be further processed, either by optical imaging technology or by analog to digital conversion and digital signal processors.

19.4.1 Coherent up or Downconversion

Phase (or time) coherent detection in the context of MMW to THz receivers is carried out by mixing the incoming field (signal) $V_s e^{i\omega_s t}$ with a high-purity reference signal (local oscillator, LO) $V_r e^{i\omega_r t}$ within a nonlinear circuit element, such as a diode. In most common situations, $V_s \ll V_r$.

Heterodyning produces an intermediate frequency (IF) signal at a frequency $\omega_{IF} = \omega_s - \omega_r \ll \omega_s, \omega_r$ with an amplitude that is multiplied by the (ideally noiseless) LO: $V_{IF} = V_r V_s$. A typical heterodyne radiometer architecture is shown in Fig. 19.7. The incoming THz field is coupled via an antenna to a waveguide incorporating the mixer. The mixer may be preceded by a low-noise amplifier (LNA), especially if the frequency is below ~ 100 GHz where integrated amplifiers are readily available. To compensate for $1/f$ noise and drifts, a so-called Dicke-switch [39] is typically placed before the mixer. The LO signal is coupled via a matching network to the mixer. Typically, the output of the mixer is filtered by a bandpass filter, which removes the upper sideband signals ($2\omega_s, 2\omega_r, \omega_s + \omega_r$). This is followed by an IF LNA, which amplifies the IF signal. Finally, the output of the IF LNA is coupled via a video filter to a detector, which converts the IF signal to baseband, i.e., the video signal and in this process the phase information is lost. The output of the video detector is now proportional to the incoming THz power. The first reported solid-state heterodyne downconversion receiver systems designed for passive MMW security imaging appeared in the early 1990s [40, 41]

Large image forming arrays of SMMW heterodyne radiometers tend to suffer from “LO starvation”: Schottky mixers typically require ~ 1 mW of LO power. Given that most available source technologies can barely produce such power levels at a few hundred GHz, a source per receiver is required. This in turn requires either a fully integrated LO source, or alternatively an efficient method of LO power distribution across the array. A solution to the former may be monolithically integrated heterodyne receiver arrays [42, 43]. The latter could be solved by the use of optically generated LO using LT-GaAs THz photomixers as per-pixel LO sources [44–46].

Coherent optical upconversion is an approach that has been investigated actively over the recent years [32, 47]. The method is an optical analog to coherent downconversion in the electrical domain. In this method, the incoming THz field is coupled via an antenna to an electro-optic modulator where it is mixed with an optical LO signal. The modulator is a device whose optical index of refraction is a function of the (THz) electric field. The THz power generates sidebands around the optical carrier frequency. The carrier is suppressed with a bandpass filter, and the sideband signals are consequently detected by a photodiode. The attractive feature of this approach lies in its ability to harness the vast array of optical telecommunications hardware readily available today and the use of fiber-optical techniques to distribute the sig-

Fig. 19.7 A typical heterodyne receiver architecture. Components that are often omitted are represented by dashed lines

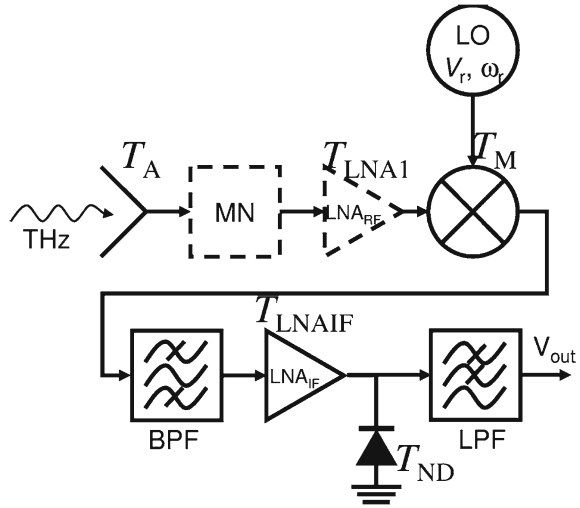
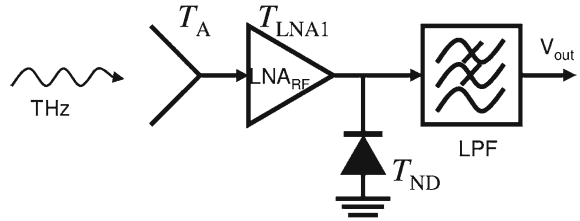


Fig. 19.8 The architecture of a preamplified direct detection receiver



nals from different channels across large distances much more easily than mm-wave signals.

19.4.2 Preamplified Direct Detection

Preamplified direct detection relies upon an LNA stage with large bandwidth which is used to “boost” the incoming electromagnetic signal above the noise of the detector that follows the LNA.

A simple schematic of the preamplified direct detection architecture is shown in Fig. 19.8. An important benefit of preamplified direct detection is that it does not require an LO source. This considerably simplifies the realization of receiver arrays. The inherent drawback is that the frequency coverage of the receiver is limited by the availability of LNA technologies to frequencies below ~ 200 GHz, a fact that at present restricts the application of this technology to short range imaging applications only due to the diffraction limit. This could well change in the future, as substantial R&D efforts are under way to develop LNAs up to 1 THz [48–50].

Until recently, the detector of choice following the LNA has been the Schottky diode. Contrarily, their excellent mixing performance in heterodyne instruments, the conventional Schottky barrier diode is a relatively poor detector: A DC bias is required to bias the diode to an impedance that can be impedance matched to the output of the LNA, and in order to gain sufficient responsivity. The DC bias gives rise to a substantial amount of $1/f$ noise, which needs to be circumvented with a Dicke switch.

Recent developments in low-barrier Schottky and zero-bias diodes [51–54] that have much lower $1/f$ noise significantly reduces the gain required from the preceding LNA stage(s): The lower the noise of the diode detector, the less amplification is required to reach a situation where the LNA noise dominates the system noise. This is highly desirable from the standpoint of system complexity and consequently, system cost [55].

All but one of the presently commercially available passive mm-wave cameras are based on preamplified direct detection arrays. Small production numbers, highly specialized fabrication processes associated with the manufacturing of MMW LNAs, and the need for accurate mounting to associated packaging (incorporating waveguides, coupling horns etc.) lead to high component costs. Thus, the design of passive systems is often a compromise between the radiometric performance (NETD scaling as $N_{\text{ch}}^{-1/2}$ due to increase in per-pixel integration time) and the cost of the camera frontend.

Efforts to reduce the per-channel cost are under way, especially focussing in the development of highly integrated receiver systems based on low cost materials such as Si and SiGe [43, 56]. The integrated receivers can potentially replace the compound semiconductor receiver technology if larger receiver counts at a competitive FPA cost can be achieved. The larger number of receivers may partly compensate for the inferior noise performance compared to higher performance InP or GaAs MMICs.

19.4.3 Incoherent (Unamplified) Direct Detection

With sensitive enough detectors, the LNA can be omitted altogether. At present, the most sensitive room temperature MMW detectors are zero-bias diodes and low-barrier Schottky diodes with NEPs around $1 \text{ pW}/\sqrt{\text{Hz}}$, improving with operating temperature and is directly proportional to T [57]. Operation in the SMMW region is possible, but the impedance matching of diodes to antennas becomes challenging. Bolometers with a NEP of $\sim 25 \text{ pW}/\sqrt{\text{Hz}}$ at room temperature [58] are readily adapted for SMMW operation. However, at the quoted NEPs, unamplified direct detectors are only applicable to active imaging, with holographic imaging as one example [59, 60]. If cooling is allowed, cryogenic bolometers ($\text{NEP} \propto T^{3/2}$ to $T^{5/2}$) and superconductor-insulator-superconductor diodes provide an alternative for passive detection. The added system backend complexity caused by the need for refrigeration is compensated by their high performance, low manufacturing cost, scalability to staring focal plane arrays, and frequency agility.

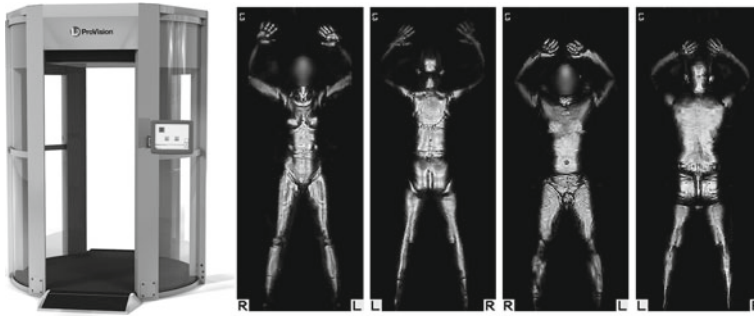


Fig. 19.9 (Left) The L-3 ProVision active mm-wave portal. (Right) 2-D projections of the volumetric data sets on two individuals (first two: *female*; last two: *male*). The faces are blurred for privacy. [61]

19.5 Millimeter-Wave Portals

In this section we give examples of some of the commercially available MMW portals, or short-range systems (typically providing still imagery).

19.5.1 L-3 ProVision

The L-3² ProVision³ system is an active holographic MMW portal, whose origins date back to the early 1990s. The technology employed in the portal was developed by Battelle Pacific Northwest Labs [62, 63], and later licensed to L-3. The system consists of a linear array of 35 GHz radar transceivers, mounted on a platform that carries out a cylindrical scan of the subject person, located on the rotation axis of the linear array. The image is formed through computational methods (FFTs). Given the ranging capability, the system provides volumetric (3D) still images of the subject. Image scan time is about 2 s, with several seconds required to compute and display the image. At present, the L-3 ProVision is globally the most widely deployed portal system (Fig. 19.9).

19.5.2 Millivision

Millivision's⁴ technology builds on arrays of preamplified direct detectors operating at 94 GHz. The Millivision Portal system 350⁵ and the Walk-by system 350 utilize

² L3 Communications <http://www.sds.l-3com.com/index.htm>.

³ ProVision® <http://www.sds.l-3com.com/advancedimaging/provision.htm>.

⁴ <http://www.millivision.com/>

⁵ <http://www.millivision.com/portal-350.html>.

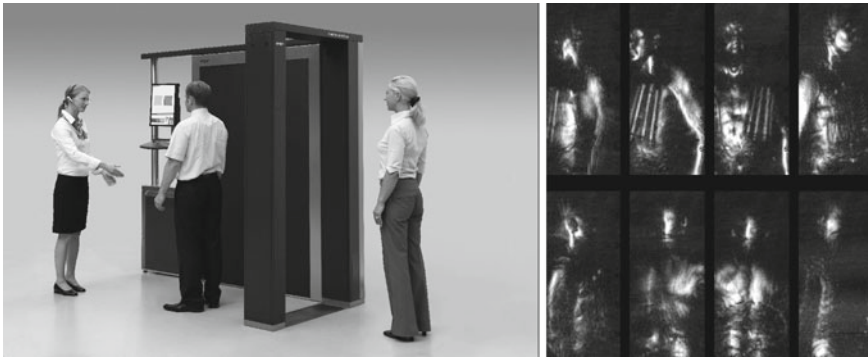


Fig. 19.10 (Left) The Smiths eqo portal. (Right) MMW imagery (frames from a movie) from the Agilent technologies prototype, an early precursor of the eqo [17]

artificial enhancement of contrast by heated or cooled panels whose temperature is substantially different from that of the ambient surroundings or the human body. The systems are also near-real time, providing about a frame rate of 10Hz. In the portal system, subject rotation by 360° yields full-body all-aspect imagery, while the walk-by system deploys two imagers (front/back) to cover both sides of the subject.

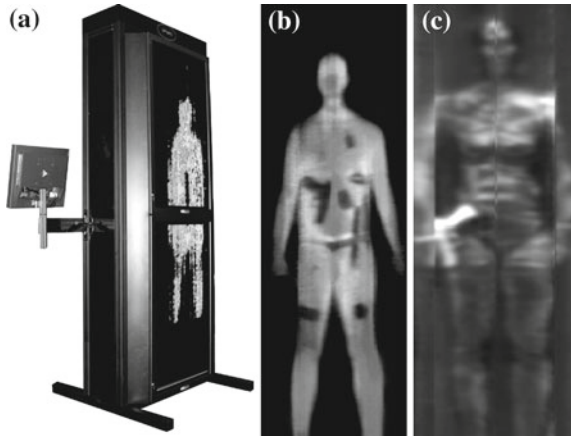
19.5.2.1 Smiths eqo

The Smiths⁶ eqo⁷ system is an active MMW portal (shown on the left in Fig. 19.10). The system is unique in the sense that it does not involve moving parts. An initial demonstrator was constructed by Agilent Technologies, and published in 2006 [17]. In the Agilent Technologies approach, image formation is carried out by reflecting a transceiver beam at 24 GHz off a digitally programmable reflector which focuses the transmitted mm-wave beam to a desired location on the target. Different “voxels” correspond to a specific digital phase pattern which is programmed onto the reflector. Thanks to the electronic scanning, only a small number of mm-wave electronic components are required, and due to the digital nature of the system it benefits from the rapid advance of digital microelectronics for the phase pattern generation subsystems. The system provides real-time video, and its highly adaptive nature does not suffer from depth-of-field issues that typically hamper the performance from imaging systems using physical lenses or mirrors.

⁶ Smiths Detection http://www.smithsdetection.com/?no_cache=1&L=4&e=1

⁷ <http://www.smithsdetection.com/eqo.php>

Fig. 19.11 **a** The Sago Systems Inc. iPat portal. **b** indoors and **c** outdoors imagery acquired with the system. (Images courtesy of C. Martin, Sago Systems, Inc.)



19.5.2.2 Sago Systems, Inc.

Sago's⁸ imaging systems utilize a linear array of preamplified direct detection receivers operating at 94 GHz. The image is formed using a clever combination of mechanical and electrical scanning [65, 66]. The benefit of Sago's approach is the small number of high frequency amplifiers required, which allows the use of state-of-the-art LNAs without compromising system cost. Near real time imaging is possible, but with degraded NETD since the system scans in both directions leaving little per-pixel integration time. Sago has built several versions of the frequency-scanned radiometers, an example of which is shown in Fig. 19.11.

19.6 Stand-off Imaging

Stand-off imaging of concealed explosives and weapons has been the focus of intensive research for several years. The technical challenges are substantial, not only due to the longer imaging distance, but also due to the fact that stand-off imaging scenarios often require video rate imaging systems in order to be able to screen moving people. This section only includes systems and prototypes that produce near-real-time imagery.

19.6.1 Passive Stand-Off Imaging Systems

The challenges associated with passive stand-off systems are mostly associated with the development of SMMW receiver arrays with sufficient sensitivity for passive detection. As described in Sect. 19.2, since passive systems rely on ambient black-

⁸ Sago Systems Inc. <http://www.trexenterprises.com/Subsidiaries/sago.html>

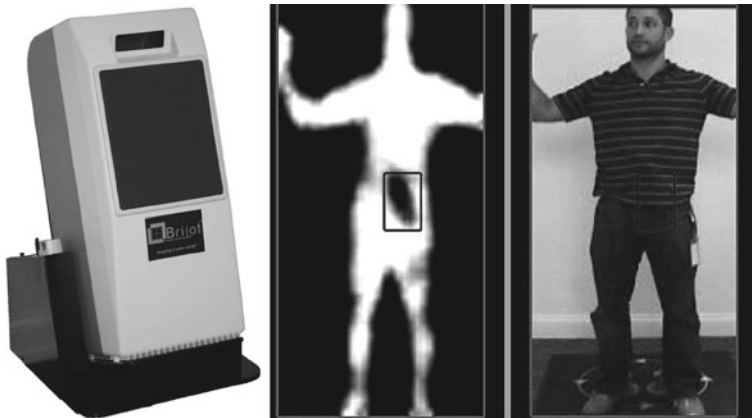


Fig. 19.12 The Brijot GEN2 passive MMW camera, and corresponding imagery. Images courtesy of Brijot Imaging Systems Inc.

body illumination they suffer from atmospheric and clothing attenuation more than their active counterparts [67].

19.6.1.1 Brijot Imaging Systems

Brijot⁹ Imaging Systems sell several product variations based on a preamplified direct detection receiver array imager operating at a center frequency of 94 GHz. The Brijot GEN2¹⁰ system (see Fig. 19.12) which incorporates mechanically scanned optics is capable of full-body imaging at 4–12 Hz frame rate with an image resolution of about 6 cm × 6 cm at a distance of 3–5 m. The company also sells solutions which include two units for simultaneous front- and backside imaging (Fig. 19.13).

19.6.1.2 Thruvision Systems

The stand-off systems from Thruvision¹¹ utilize an 8-channel heterodyne down-conversion receiver operating at 250 GHz, coupled with reflective telescopic optics intended for imaging from 3 m up to ~25 m. The T5000¹² is essentially a ruggedized version of the T4000¹³ system, intended for outdoors use. The T4000 angular

⁹ Brijot® is now MicroSemi <http://www.brijot.com/>

¹⁰ GEN2 ® <http://www.brijot.com/products/gen2>

¹¹ Thruvision has been acquired by Digital Barriers <http://www.thruvision.com/>

¹² Has become TS4 http://www.thruvision.com/Products/TS4_Sub_Pages/TS4_Product_Page.htm

¹³ TS5 http://www.thruvision.com/Products/TS5_Sub_Pages/TS5_Product_Page.htm

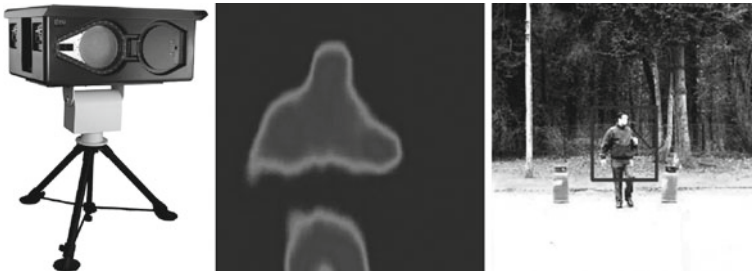


Fig. 19.13 The Thruvision T5000 ruggedized camera, and corresponding imagery

resolution (defined as the full width at half maximum of the Gaussian point spread function) and angular FOV are $\sim 1.26^\circ$ and $18.9^\circ(\text{H}) \times 24.8^\circ(\text{V})$, respectively. For the T5000, the numbers are $\sim 1.0^\circ$ and $17.3^\circ(\text{H}) \times 15.5^\circ(\text{V})$. Thruvision also offers a portal system, the T8000. Image acquisition time is variable from 3 to 30 s, with a spatial resolution of $20 \text{ mm} \times 20 \text{ mm}$.

19.6.1.3 VTT/NIST Passive THz Camera

The use of cryogenically cooled bolometer arrays as sensitive SMMW detectors may offer a solution for stand-off imaging. While the need for cooling brings about several other issues, such as the need for a cryocooler, the necessary cool down time for operations and larger weight and power consumption, this approach nevertheless has shown some promise in providing a route in the near term future for stand-off imaging.

A research prototype system developed jointly by Aalto University, NIST, and VTT is a broadband incoherent system that utilizes superconducting antenna-coupled microbolometers [68] configured in a linear array [69, 70]. The electrical NEP of these sensors is $\sim 8 \times 10^{-15} \text{ W}/\sqrt{\text{Hz}}$. The detector array is mounted onto the second stage of a commercial pulse tube cryocooler, and is operated at temperatures between 4 K and 7 K. The benefit of a pulse tube cooler is its high reliability and long maintenance period ($\sim 20\,000 \text{ h}$).

The nominal design bandwidth of the detectors is from 200 GHz to 1 THz, and the effective center frequency of 640 GHz has been inferred from detector beam pattern measurements. The image is formed using a folded, all-reflective variant of the Schmidt telescope that provides a large FOV. A periscopic conical scanner allows for the formation of a 2D image at frame rates up to about 10 Hz. At 7 Hz, the system NETD has been measured to be $\sim 0.5 \text{ K}$ with a spatial resolution of $(4 \text{ cm})^2$ at a focus distance of 5 m. The spatial resolution is limited by the sampling of the image, a tradeoff between the number of detectors in the linear array and the relatively large angular FOV of $\pm 15^\circ(\text{H})$ by $\pm 7.5^\circ(\text{V})$.

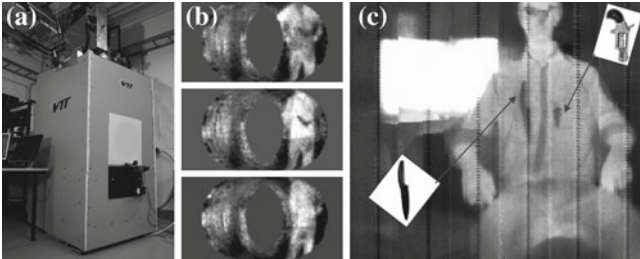


Fig. 19.14 **a** An image of the passive video-rate THz camera. **b** Three frames from a passive THz video acquired at frame rate of 7 Hz at 5 m focus distance, with the top frame showing a person concealing a gun under fleece jacket, center frame with the jacket opened, and bottom frame showing a wallet in the back left pocket of trousers. The hole in the center of the field is only due to partly filled linear detector array; **c** Raster-scanned still image taken with a similar detector array, acquired at 2.5 m focus distance. Image acquisition time was 2 min

An image of the system, SMMW frames from a movie and still images taken with a similar system are shown in Fig. 19.14. A smaller version of the system with improved sampling (and a smaller FOV), along with a multi-spectral version are under development.

19.6.1.4 Jena/IPHT Safe-Visitor

The SAFE-VISITOR passive camera prototype also utilizes cryogenic microbolometers [8, 71]. The sensors are configured in a circular array of 20 detectors and are operated within a commercial dry $^4\text{He}/^3\text{He}$ sorption cooler at a bath temperature of 0.3 K. As bolometers improve quickly with temperature, the electrical NEP of the bolometers is $\sim 1 \times 10^{-16} \text{ W}/\sqrt{\text{Hz}}$. In comparison with the system described in 19.6.1.3, the benefit of the excellent NEP is twofold: (i) it requires a smaller number of detectors to sample an image at a given required NETD and frame rate and (ii) it allows for smaller THz bandwidth, simplifying optics design and reducing the effect of clothing attenuation. These benefits are however counterbalanced by the lower bath temperature requirement, necessitating the use of a more expensive sorption cooler that requires an automated regeneration cycle of 2 h every 24 h (Fig. 19.15).

The image is formed using a Cassegrain telescope with an aspherical primary mirror, and a spiral-scanning secondary. The optical configuration is quite compact, a common merit of the Cassegrain telescope, but it has a somewhat limited radial FOV of 5° , corresponding to 1.6–10 m. The system design bandwidth is from 335 to 375 GHz, defined by a set of bandpass filters, and it can be run at frame rates up to 10 Hz.

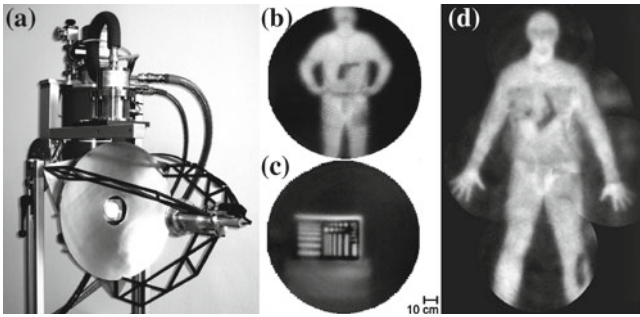


Fig. 19.15 **a** An image of the SAFE-VISITOR system **b** a passive image of a person with a mock-up gun at 8 m stand-off **c** a passive image of a resolution target at 8 m **d** a full-body montage from several smaller FOV images at 5 m (taken with a laboratory pre-cursor system) [8, 71]

19.6.2 Active Stand-Off Imaging Systems

Active stand-off imaging systems employ an artificial source of radiation that is used to illuminate the target, located at a distance from the source and the detector. The primary benefits of active imaging are those described in Sect. 19.2.

19.6.2.1 Imaging SMMW Radar Systems

Among promising candidates for active stand-off imaging are the 350 GHz and 675 GHz frequency-modulated continuous-wave (FMCW) radar imagers developed by PNNL and JPL, respectively [18, 19]. The ranging capability is of great importance, as it avoids the strong first-surface (clothing) reflections to reveal the much weaker signatures beneath the clothes [72]. The JPL system consists of a conventional (albeit very high frequency) monostatic low-power ($250 \mu\text{W}$) radar frontend that is frequency-swept across 662–688 GHz, yielding a theoretical range resolution of ~ 6 mm. Because of the high center frequency, the 26 GHz bandwidth corresponds to only $\sim 4\%$ relative bandwidth, allowing for straightforward implementation of the RF and scanning optics components. The system has been demonstrated in the imaging of concealed objects at a record stand-off range of 25 m at a frame rate of 0.2 Hz (see Fig. 19.16). At present, the system can only cover a relatively small FOV of $50\text{ cm} \times 50\text{ cm}$, limited by the optomechanical scanning and the chirp generator.

The PNNL system transmits approximately 4 mW, chirped from 340 GHz to 360 GHz, corresponding to a range resolution of 8 mm. The radar is coupled to conical scanning optics designed for stand-off ranges of 2 m, 5 m, and 10 m with a full-body FOV and an image acquisition time of ~ 10 s. Sample images are shown in 19.4d and e. In the case of both systems, full-body coverage at video rates requires substantial development efforts, especially if multi-channel transceiver systems are

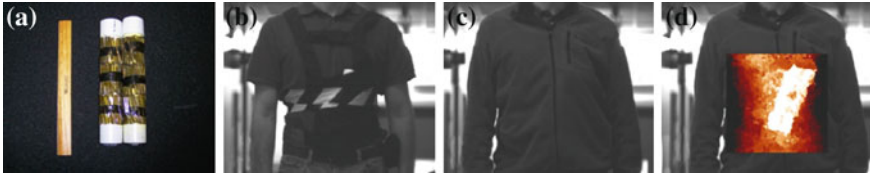


Fig. 19.16 Target scenario and SMMW image overlay for through-jacket detection of a mock pipe bomb. The image was acquired in 5 s at a range of 25 m. **a** Mock pipe bomb **b** the bomb strapped to torso **c** jacket covering the threat **d** SMMW image overlay. Image adapted from [19]

required for real-time imaging. Steps toward such architectures have already been undertaken [73].

19.7 Multispectral and Spectroscopic Imaging

As discussed in Sect. 19.2, properties of materials are frequency dependent. The transmission/absorptivity, emissivity, reflectivity, and scattering of objects of interest, background, and barriers all change with frequency. This leads to the possibility of combining images at several frequencies in order to improve image contrast, in just the same way as a color photograph often reveals more information than black and white images.

In the THz region (above 600 GHz or so), it was found in the early 2000s that many common explosives exhibit characteristic absorption lines in their THz spectra. This offers the intriguing possibility that THz spectroscopy could be used as a safe method of detecting and identifying explosives concealed on the body.

19.7.1 Multispectral Imaging

Kemp et al. [74, 75] have shown how multi-spectral imaging can greatly improve the interpretation of B-scan images – see Fig. 19.17. Here, the broadband image shows a B-scan depth slice through a number of test objects covered with cloth. The multispectral image separates the image into three frequency bands (0.5–0.7; 0.7–1.0; and, 1.0–3.0 THz) which are colored red, green, and blue, respectively, and then recombined into a false-color image. This reveals differences between the test objects due to the way they absorb high frequencies and texture in the cloth which is largely due to scattering.

Overall, there has been relatively little work carried out in this area. This is probably due to the cost and complexity of developing imaging systems which operate at two or more frequencies.

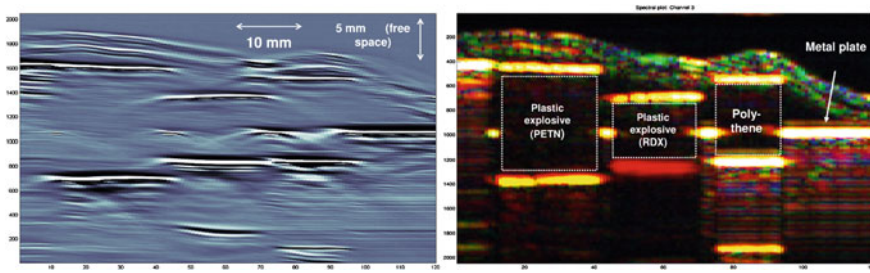


Fig. 19.17 Broadband and multispectral THz *B*-scan images of a number of objects hidden beneath two layers of cloth

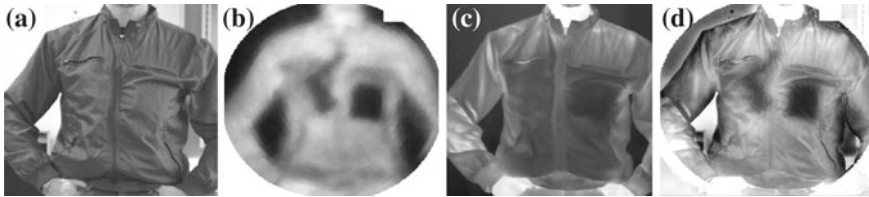


Fig. 19.18 Image fusion example from the Safe VISITOR project: **a** visible image **b** THz image **c** infrared image **d** fused image [8, 71]

Grossman et al. at NIST [76] developed a rotating frequency-selective filter wheel which could be used in front of a broadband microbolometer imager for multispectral imaging. The bolometric cameras detailed in Sect. 19.6 could be readily adapted for multi-frequency detection given the frequency-agility of bolometers.

Of course, multispectral imaging need not be restricted to MMW-THz frequencies alone: infrared thermal imaging can be used to infer the presence of hidden objects through the way they block heat conduction to the surface; infrared and visible wavelength imaging can help distinguish the outline of the body from the background and provide surface detail to facilitate interpretation. The fusion of visible, infrared, and MMW images has been explored since the earliest days of MMW imaging for security [77] and is used in a number of commercial products. Fig. 19.18 shows an example.

19.7.2 THz Spectroscopic Imaging

The THz spectra of common energetic compounds (RDX, PETN, HMX, TNT) and commercial explosives based on these compounds (PE4, Semtex-H) were first reported in 2003 [78]. These results are shown in Fig. 19.19 and have subsequently been validated and extended by a number of groups [79–83] using time domain THz spectroscopy and FTIR. The strong absorption features, particularly of RDX-based explosives around 800 GHz, appear to open up the possibility of material-specific

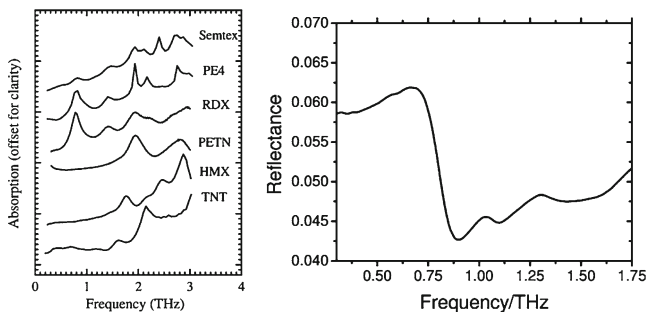


Fig. 19.19 (Left) THz transmission spectra of the raw explosive materials TNT, HMX, PETN, and RDX together with the spectra of the compound explosives PE4 and Semtex H. (Right) Reflection spectrum of the explosive Semtex H [85]

detection of these materials. These features are relatively distinct from harmless, potential confusion, and barrier materials. Kawase [84] has also identified strong signatures in a number of drugs of abuse and cutting agents.

Practical detection systems will need to operate in reflection rather than transmission mode due to the high absorption coefficients of the explosives themselves and, for people screening applications, due to absorption by the body. Fig. 19.19 shows the reflection spectrum of Semtex H, a mixture of RDX and PETN; the spectral features due to the resonances are still visible, but are much weaker when measured in reflection geometry measurements. The spectral features are also present in scattered radiation, but here the overall signal strength is several orders of magnitude lower, again making detection more challenging. Laboratory experiments have demonstrated real-time detection of RDX-based explosives at modest stand-off distances around 1 m [85] using smooth, flat samples, and specular reflection. Spectroscopic imaging has also been demonstrated in the laboratory [86]. It continues to prove extremely challenging, however, to progress beyond this toward a system which could be deployed on the wide variety of configurations that would be met in any practical deployment. Scattering from explosives and clothing causes significant measurement artifacts [87, 88] and the strong absorption from clothing at frequencies of 2 THz and above, which are needed to see many of the spectral features, means that the signal becomes lost in the noise. Doubts have been raised over whether practical systems will ever be achieved [89].

19.8 Future Directions

MMW portals have matured to the point where the next steps will be associated with backend processing, such as automated target recognition (ATR) algorithms that would substantially reduce the manpower cost of operating these systems. Also the privacy issues that have been associated with active MMW portals will be remediated by ATR. Systems such as the L-3 ProVision have already started deploying systems

with ATR features. For the short-range stand-off passive MMW imagers the major driver will be to reduce system costs. Significant cost reductions will be enabled through, lower cost receiver technology, new packaging solutions, and semiconductor process developments that may include the development of integrated receiver front ends incorporating either new materials, e.g., SiGe, InSb, or InP LNAs with Si backend circuitry.

In addition to cost reductions, major improvements in system performance are still required, especially for medium to long-range stand-off imaging. Component technology for room-temperature SMMW systems either does not exist or is far too expensive for passive imaging. Future innovations in, e.g., THz LNA, oscillator, and integrated heterodyne receiver development are likely, albeit the cost of the technology may remain high for several years. Cryogenic imagers are possibly at the highest technology readiness level with respect to passive SMMW imaging, but this approach has to be proven in the field in order to show that the benefits outweigh the costs of cooling.

The most promising route for long-range stand-off imaging is through active SMMW radar imaging. The primary challenge is to increase the frame rate of these systems to near-real-time and full-body coverage. Given the cost of the SMMW front end components, brute force scale-up to multi-channel receivers will be expensive. Alternatives are provided through the development of rapid, electronic beam steering technology combined with higher power sources.

Interestingly, the field is also seeing product differentiation as systems vendors are beginning to provide systems tailored for various operational scenarios, creating a range of products. Furthermore, a major trend in security technology is the progress toward systems of systems, i.e., multi-sensory solutions in which the MMW or SMMW imaging systems complement other orthogonal sensors. This is likely to produce highly effective, comprehensive security screening solutions, neither MMW nor SMMW imaging provides a “silver bullet” to counter threats.

Spectroscopic imaging, or multi-color THz imaging remains an intriguing possibility that could enable better discrimination of hazardous items, but will certainly not provide a high degree of specificity due to the atmospheric and clothing extinction, as well as the fact that the THz resonances of solid and liquid materials at ambient conditions are broad, making them difficult to discriminate from the background.

Finally, it is worth noting that while much of the systems development in the past few years has been very much security applications driven, the by-product has been a completely new set of tools for observing the world within the least well-known range of the electro-magnetic spectrum for many other applications.

References

1. R.M. Granham, N.T.W. Graham, Flight trials with the green minnow equipment. RRE memorandum 1461, Royal Radar Establishment, 1958
2. D.T. Hodges, E.E. Reber, F.B. Foote, Safeguards applications of far infrared radiometric techniques for the detection of contraband. *J. Nucl. Mater. Manag.* **9**(4), 83 (1980)

3. E.E. Reber, F.B. Foote, R.L. Schellenbaum, R.G. Bradley, Evaluation of active and passive near millimeter-wave radiometric imaging techniques for detection of concealed objects. Department of Commerce National Technical Information Service DE81 031 938, Sandia National Laboratories, July 1981
4. http://en.wikipedia.org/wiki/Receiver_operating_characteristic
5. F.T. Ulaby, R.K. Moor, A.K. Fung, *Microwave Remote Sensing - Active and Passive*, vol. 1 (Microwave Remote Sensing Fundamentals and Radiometry, Artech House, 1981)
6. N.A. Salmon, Polarimetric scene simulation in millimeter-wave radiometric imaging. *SPIE* **5410**, 260–269 (2004)
7. C.A. Martin, J.A. Lovberg, W.H. Dean, E. Ibrahim, High-resolution passive millimeter-wave security screening using few amplifiers. *SPIE* **6548**, 654806 (2007)
8. T. May, G. Zieger, S. Anders, V. Zakosarenko, H.-G. Meyer, M. Schubert, M. Starkloff, M. Rößler, G. Thorwirth, U. Krause, Safe visitor: visible, infrared, and terahertz object recognition for security screening application. *SPIE* **7309**, 73090E (2009)
9. D.T. Petkie, C. Casto, F.C. De Lucia, S.R. Murrill, B. Redman, R.L. Espinola, C.C. Franck, E.L. Jacobs, S.T. Griffin, C.E. Halford, J. Reynolds, S. O'Brien, D. Tofsted, Active and passive imaging in the THz spectral region: phenomenology, dynamic range, modes, and illumination. *J. Opt. Soc. Am. B* **25**(9), 1523–1531 (2008)
10. A. Luukanen, L. Grönberg, T. Haarnoja, P. Helistö, K. Kataja, M. Leivo, A. Rautiainen, J. Penttilä, J.E. Bjarnason, C.R. Dietlein, M.D. Ramirez, E.N. Grossman, Passive THz imaging system for stand-off identification of concealed objects: results from a turn-key 16 pixel imager. *SPIE* **6948**, 69480O (2008)
11. N.A. Salmon, R. Appleby, P.R. Coward, Polarimetric millimeter-wave imaging. *SPIE* **4373**, 82–85 (2001)
12. G.N. Sinclair, R.N. Anderton, R. Appleby, Passive millimeter-wave concealed weapon detection. *SPIE* **4232**, 142–151 (2001)
13. P.R. Coward, R. Appleby, Development of an illumination chamber for indoor millimeter-wave, imaging. *SPIE* **5077**(1), 54–61 (2003)
14. R. Doyle, B. Lyons, A. Lettington, T. McEnroe, J. Walshe, J. McNaboe, P. Curtin, Illumination strategies to achieve effective indoor millimeter wave imaging for personnel screening applications. *SPIE* **5789**(1), 101–108 (2005)
15. F.T. Ulaby, R.K. Moor, A.K. Fung, *Microwave Remote Sensing - Active and Passive, Vol. II, Radar Remote Sensing and Surface Scattering and Emission Theory*, Artech House, 1982
16. D.M. Sheen, D.L. McMakin, T.E. Hall, Cylindrical millimeter-wave imaging technique and applications. *SPIE* **6211**, 62110A (2006)
17. P. Corredoura, Z. Baharav, B. Taber, G. Lee, Millimeter-wave imaging system for personnel screening: scanning 10^7 points a second and using no moving parts. *SPIE* **6211**, 62110B (2006)
18. D.M. Sheen, T.E. Hall, R.H. Severtsen, D.L. McMakin, B.K. Hatchell, P.L.J. Valdez, Standoff concealed weapon detection using a 350-GHz radar imaging system. *SPIE* **7670**, 767008 (2010)
19. K.B. Cooper, R.J. Dengler, N. Llombart, A. Talukder, A.V. Panangadan, C.S. Peay, I. Mehdi, P.H. Siegel, Fast high-resolution terahertz radar imaging at 25 meters. *SPIE* **7671**, 76710Y (2010)
20. D.M. Sheen, D.L. McMakin, W.M. Lechelt, J.W. Griffin, Circularly polarized millimeter-wave imaging for personnel screening. *SPIE* **5789**, 117–126 (2005)
21. M.J. Rosker, H.B. Wallace, Imaging through the atmosphere at terahertz frequencies. in *Proceedings of IEEE/MTT-S International Microwave, Symposium*, pp. 773–776 2007
22. J.E. Bjarnason, T.L.J. Chan, A.W.M. Lee, M.A. Celis, E.R. Brown, Millimeter-wave, terahertz, and mid-infrared transmission through common clothing. *Appl. Phys. Lett.* **85**(4), 519–521 (2004)
23. N.E. Alexander, C.C. Andrés, R. Gonzalo, Multispectral mm-wave imaging: materials and images. *SPIE* **6948**, 694803 (2008)
24. M.R. Leahy-Hoppa, M.J. Fitch, X. Zheng, L.M. Hayden, R. Osiander, Wideband terahertz spectroscopy of explosives. *Chem. Phys. Lett.* **434**(4–6), 227–230 (2007)

25. M.J. Fitch, M.R. Leahy-Hoppa, E.W. Ott, R. Osiander, Molecular absorption cross-section and absolute absorptivity in the THz frequency range for the explosives TNT, RDX, HMX, and PETN. *Chem. Phys. Lett.* **443**, 284–288 (2007)
26. A.D. Burnett, W.H. Fan, P.C. Upadhy, J.E. Cunningham, H.G.M. Edwards, J. Kendrick, T. Munshi, M. Hargreaves, E.H. Linfield, A.G. Davies, Broadband terahertz time-domain and raman spectroscopy of explosives. *SPIE* **6549**, 654905 (2007)
27. R. Appleby, H.B. Wallace, Standoff detection of weapons and contraband in the 100 GHz to 1 THz, region. **55**(11), 2944–2956 (2007)
28. P. Goldsmith, *Quasioptical Systems : Gaussian Beam Quasioptical Propagation and Applications*. IEEE, 1998
29. P.F. Goldsmith, Quasi-optical techniques. *Proc. IEEE* **80**(11), 1729–1747 (1992)
30. N.A. Salmon, J. Beale, J. Parkinson, S. Hayward, P. Hall, R. Macpherson, R. Lewis, A. Harvey, Digital beam-forming for passive millimetre wave security imaging. in *Proceedings of Second European Conference Antennas and Propagation EuCAP 2007*, pp. 1–11, 2007
31. J. Christensen, A. Carlström, A. Emrich, P. de Maagt, Spaceborne submm-wave interferometry. in *Proceedings of IEEE Antennas and Propagation Society International Symposium 2006*, pp. 2387–2390, 2006
32. C.A. Schuetz, J. Murakowski, G.J. Schneider, D.W. Prather, Radiometric millimeter-wave detection via optical upconversion and carrier suppression. *IEEE Trans. Microwave Theor. Techniques* **53**(5), 1732–1738 (2005)
33. H. Kamoda, T. Iwasaki, J. Tsumochi, T. Kuki, 60-GHz electrically reconfigurable reflectarray using p-i-n diode. in *Proceedings of IEEE MTT-S International Microwave Symposium Digest MTT '09*, pp. 1177–1180, 2009
34. A. Moessinger, S. Dieter, W. Menzel, S. Mueller, R. Jakoby, Realization and characterization of a 77 GHz reconfigurable liquid crystal reflectarray. in *Proceedings of 13th International Symposium Antenna Technology and Applied Electromagnetics and the Canadian Radio Science Meeting ANTEM/URSI 2009*, pp. 1–4, 2009
35. M.R. Chaharmir, J. Shaker, M. Cuhaci, A.-R. Sebak, Novel photonically-controlled reflectarray antenna. *IEEE T Antenn. Propag.* **54**(4), 1134–1141 (2006)
36. P.H. Siegel, Terahertz technology. *IEEE Trans. Microwave Theor. Tech.* **50**(3), 910–928 (2002)
37. E.R. Brown, Fundamentals of terrestrial millimeter-wave and THz remote sensing. *Int. J. High Speed Electron. Syst.* **13**, 995–1097 (2003)
38. P. Siegel, R. Dengler, Terahertz heterodyne imaging part ii: Instruments. *Int. J. Infrared Millimeter Waves* **27**, 631–655 (2006). 10.1007/s10762-006-9109-4
39. R.H. Dicke, The measurement of thermal radiation at microwave frequencies. *Rev. Sci. Instrum.* **17**(7), 268–275 (1946)
40. P.F. Goldsmith, C.-T. Hsieh, G.R. Huguenin, J. Kapitzky, E.L. Moore, Focal plane imaging systems for millimeter wavelengths. *IEEE Trans. Microwave Theor. Tech.* **41**(10), 1664–1675 (1993)
41. G.R. Huguenin, Millimeter wave focal plane array imager. *SPIE* **2211**, 300–301 (1994)
42. C. Jung, C. Lee, B. T., G. Chattopadhyay, A. Peralta, R. Lin, J. Gill, I. Mehdi, Silicon micro-machining technology for THz applications. in *35th International Conference on Infrared Millimeter and Terahertz Waves (IRMMW-THz)*, pp. 1–3, 2010
43. U.R. Pfeiffer, E. öjefors, Terahertz imaging with cmos/bicmos process technologies. in *Proceedings of ESSCIRC*, pp. 52–60, 2010
44. E.K. Duerr, K.A. McIntosh, S.M. Duffy, S.D. Calawa, S. Verghese, C.-Y.E. Tong, R. Kimberk, R. Blundell, Demonstration of a 630-GHz photomixer used as a local oscillator. in *Proceedings of IEEE MTT-S International Microwave Symposium Digest*, vol 1, 127–130, 1999
45. P.G. Huggard, L. Azcona, B.N. Ellison, P. Shen, N.J. Gomes, P.A. Davies, Application of 1.55 & μm photomixers as local oscillators & noise sources at millimetre wavelengths. in *Proceedings of Conference Infrared and Millimeter Waves and 12th International Conference Terahertz Electronics Digest of the 2004 Joint 29th International Conference*, pp. 771–772, 2004
46. T. Noguchi, A. Ueda, Y. Sekimoto, S. Asayama, M. Ishiguro, Photonic local oscillator for sis mixers. in *Proceedings of 18th Annual Meeting of the IEEE Lasers and Electro-Optics Society LEOS 2005*, pp. 171–172, 2005

47. A.R. Harvey, P.M. Blanchard, G.M. Smith, K. Webster, A.H. Greenaway, Optical up-conversion for passive millimeter-wave imaging. *SPIE* **3064**, 98–109 (1997)
48. D. Pukala, L. Samoska, T. Gaier, A. Fung, X.B. Mei, W. Yoshida, J. Lee, J. Uyeda, P.H. Liu, W.R. Deal, V. Radisic, R. Lai, Submillimeter-wave InP mmic amplifiers from 300–345 GHz. *IEEE Microw Wirel Co.* **18**(1), 61–63 (2008)
49. I. Kallfass, A. Tessmann, A. Leuther, H. Massler, M. Schlechtweg, O. Ambacher, Millimeter-wave monolithic integrated circuits for imaging and remote sensing at 140, 200, and 300 GHz. *SPIE* **7485**, 74850L (2009)
50. W.R. Deal, X.B. Mei, V. Radisic, K. Leong, S. Sarkozy, B. Gorospe, J. Lee, P.H. Liu, W. Yoshida, J. Zhou, M. Lange, J. Uyeda, R. Lai, Demonstration of a 0.48 THz amplifier module using InP HEMT transistors. *IEEE Microwave Wirel. Compon. Lett.* **20**(5), 289–291 (2010)
51. J.N. Schulman, T.Y. Hsu, H.P. Moyer, J.J. Lynch, $1/f$ noise of sb-heterostructure diodes for pre-amplified detection. *IEEE Microwave Wirel. Compon. Lett.* **17**(5), 355–357 (2007)
52. E.R. Brown, A.C. Young, J. Zimmerman, H. Kazemi, A.C. Gossard, Advances in schottky rectifier performance. *IEEE Microwave Mag.* **8**(3), 54–59 (2007)
53. J.L. Hesler, T.W. Crowe, Nep and responsivity of thz zero-bias schottky diode detectors. in *Proceedings of and the 2007 15th Int Infrared and Millimeter Waves Conference Terahertz Electronics. IRMMW-THz. Joint 32nd International Conference*, pp. 844–845, 2007
54. D. Schoenherr, C. Bleasdale, T. Goebel, C. Sydlo, H.L. Hartnagel, R. Lewis, P. Meissner, Extremely broadband characterization of a schottky diode based THz detector. in *35th International Conference on Infrared Millimeter and Terahertz Waves (IRMMW-THz)*, pp. 1–2, 2010
55. J.J. Lynch, P.A. Macdonald, H.P. Moyer, R.G. Nagele, Passive millimeter wave imaging sensors for commercial markets. *Appl. Opt.* **49**(19), E7–E12 (2010)
56. J.W. May, G.M. Rebeiz, Design and characterization of w-band SiGe RFICs for passive millimeter-wave imaging. *IEEE Trans. Microwave Theor. Techniques* **58**(5), 1420–1430 (2010)
57. J.N. Schulman, K.S. Holabird, D.H. Chow, H.L. Dunlap, S.T., E.T. Croke, Temperature dependence of sb-heterostructure millimetre-wave diodes. *Electron. Lett.* **38**(2), 94–95 (2002)
58. A.J. Miller, A. Luukanen, E.N. Grossman, Micromachined antenna-coupled uncooled microbolometers for terahertz imaging arrays. *SPIE* **5411**, 18–24 (2004)
59. N.H. Farhat, W.R. Guard, Holographic imaging at 70 GHz. *Proc. IEEE* **58**(12), 1955–1956 (1970)
60. A. Tamminen, J. Ala-Laurinaho, A.V. Raisanen, Indirect holographic imaging at 310 GHz. *Proc. Eur. Radar Conf. EuRAD* **2008**, 168–171 (2008)
61. L-3 SafeView. <http://www.safe-view.com/ch/advancedimaging/L-3last> accessed 8th Feb 2010
62. D.L. McMakin, D.M. Sheen, H.D. Collins, T.E. Hall, R.R. Smith, Millimeter-wave high-resolution holographic surveillance system. *SPIE* **2092**, 525–535 (1994)
63. D.L. McMakin, D.M. Sheen, A. Schur, W.M. Harris, G.F. Piepel, Initial test and evaluation of the millimeter-wave holographic surveillance system. *SPIE* **2932**, 103–114 (1997)
64. <http://www.millivision.com/>, last accessed 10th February, 2011
65. J.A. Lovberg, C. Martin, V. Kolinko, Video-rate passive millimeter-wave imaging using phased arrays. in *Proceedings of IEEE/MTT-S International Microwave, Symposium*, pp. 1689–1692, 2007
66. C.A. Martin, C.E. García González, V.G. Kolinko, J.A. Lovberg, Rapid passive mmw security screening portal. *SPIE* **6948**, 69480J (2008)
67. H.B. Wallace, Analysis of rf imaging applications at frequencies over 100GHz. *Appl. Opt.* **49**(19), E38–E47 (2010)
68. A. Luukanen, J.P. Pekola, A superconducting antenna-coupled hot-spot microbolometer. *Appl. Phys. Lett.* **82**, 3970–3972 (2003)
69. A. Luukanen, L. Grönberg, M. Grönholm, P. Lappalainen, M.M. Leivo, A. Rautiainen, A. Tamminen, J. Ala-Laurinaho, C.R. Dietlein, E.N. Grossman, Real-time passive terahertz imaging system for standoff concealed weapons imaging. *SPIE* **7670**, 767004 (2010)
70. E. Grossman, C.R. Dietlein, J. Ala-Laurinaho, M.M. Leivo, L. Grönberg, M. Grönholm, P. Lappalainen, A. Rautiainen, A. Tamminen, A. Luukanen, Passive terahertz camera for standoff security screening. *Appl. Opt.* **49**(19), E106–E120 (2010)

71. E. Heinz, D. Born, G. Zieger, T. May, T. Krause, A. Krüger, M. Schulz, S. Anders, V. Zakosarenko, H.-G. Meyer, M. Starkloff, M. Rößler, G. Thorwirth, U. Krause, Progress report on Safe VISITOR approaching a practical instrument for terahertz security screening. *SPIE* **7670**, 767005 (2010)
72. K.B. Cooper, R.J. Dengler, N. Llobart, T. Bryllert, G. Chattopadhyay, E. Schlecht, J. Gill, C. Lee, A. Skalare, I. Mehdi, P.H. Siegel, Concealed object contrast enhancement using radar methods in a submillimeter-wave active imager. in *Proceedings of 33rd International Conference Infrared, Millimeter and Terahertz Waves IRMMW-THz 2008*, pp. 1–2, 2008
73. C. am Weg, W. von Spiegel, R. Henneberger, R. Zimmermann, T. Loeffler, H. Roskos, Fast active THz cameras with ranging capabilities. *J. Infrared Millimeter Terahertz Waves* **30**, 1281–1296 (2009). 10.1007/s10762-009-9565-8
74. M.C. Kemp, A. Glauser, C. Baker, Recent developments in people screening using terahertz technology: seeing the world through terahertz eyes. *SPIE* **6212**, 62120T (2006)
75. M.C. Kemp, A. Glauser, C. Baker, Multi-spectral terahertz imaging using reflected and scattered radiation. *Int. J. High Speed Electron. Syst.* **17**, 403–414 (2007)
76. E.N. Grossman, C.R. Dietlein, J. Chisum, A. Luukanen, J.E. Bjarnason, E.R. Brown, Spectral decomposition of ultra-wide-band terahertz imagery. *SPIE* **6548**, 654807 (2007)
77. N.C. Currie, F.J. Demma Jr, D.D. Ferris, R.W. McMillan, M.C. Wicks, K. Zyga, Imaging sensor fusion for concealed weapon detection. *SPIE* **2942**, 71–81 (1997)
78. M.C. Kemp, P.F. Taday, B.E. Cole, J.A. Cluff, A.J. Fitzgerald, W.R. Tribe, Security applications of terahertz technology. *SPIE* **5070**, 44–52 (2003)
79. K. Yamamoto, M. Yamaguchi, F. Miyamaru, M. Tani, M. Hangyo, T. Ikeda, A. Matsushita, K. Koide, M. Tatsuno, Y. Minami, Noninvasive Inspection of C-4 Explosive in Mails by Terahertz Time-Domain Spectroscopy. *Japanese J. Appl. Phys.* **43**, L414–L417 (2004)
80. D.J. Cook, B.K. Decker, G. Maislin, M.G. Allen, Through container THz sensing: applications for explosives screening. *SPIE* **5354**, 55–62 (2004)
81. Y. Shen, P.F. Taday, M.C. Kemp, Terahertz spectroscopy of explosive materials. *SPIE* **5619**, 82–89 (2004)
82. F. Huang, B. Schulkin, H. Altan, J.F. Federici, D. Gary, R. Barat, D. Zimdars, M. Chen, D.B. Tanner, Terahertz study of 1,3,5-trinitro-s-triazine by time-domain and fourier transform infrared spectroscopy. *Appl. Phys. Lett.* **85**(23), 5535–5537 (2004)
83. W.R. Tribe, D.A. Newnham, P.F. Taday, M.C. Kemp, Hidden object detection: security applications of terahertz technology. *SPIE* **5354**, 168–176 (2004)
84. K. Kawase, Y. Ogawa, Y. Watanabe, H. Inoue, Non-destructive terahertz imaging of illicit drugs using spectral fingerprints. *Opt. Express* **11**(20), 2549–2554 (2003)
85. C. Baker, W.R. Tribe, T. Lo, B.E. Cole, S. Chandler, M.C. Kemp, People screening using terahertz technology (invited paper). *SPIE* **5790**, 1–10 (2005)
86. Y.C. Shen, T. Lo, P.F. Taday, B.E. Cole, W.R. Tribe, M.C. Kemp, Detection and identification of explosives using terahertz pulsed spectroscopic imaging. *Appl. Phys. Lett.* **86**(24), 241116 (2005)
87. D.M. Sheen, D.L. McMakin, T.E. Hall, Speckle in active millimeter-wave and terahertz imaging and spectroscopy. *SPIE* **6548**, 654809 (2007)
88. M. Theuer, G. Torosyan, J. Jonuscheit, R. Beigang, Terahertz reflection spectroscopy for stand-off detection of explosives. in *Terahertz Wave Technology for Standoff Detection of Explosives and other Military and Security Applications*, volume SET-129. NATO Research and Technology Organisation, 2008
89. M.C. Kemp, Explosives detection using terahertz spectroscopy—a bridge too far? *IEEE TRANS. TERAHERTZ SCI. TECH.* **1**(1), 282–292 (2011)